

1 **Wind and Rain Losses for Metal-clad Contemporary Houses Subjected**
2 **to Non-cyclonic Windstorms**

3 **Hao Qin* , Mark G. Stewart**

4 Centre for Infrastructure Performance and Reliability
5 The University of Newcastle, New South Wales, 2308, Australia

6
7 17 October 2019

8 Preprint submitted to *Structural Safety*

9 **Abstract**

10 Severe windstorms cause millions in losses annually for housing in Southeast Australia that
11 has more than half of Australia's population. The risk assessment for housing in these non-
12 cyclonic regions is the key to assessing the cost-effectiveness of relevant wind mitigation
13 measures to reduce the economic losses. This study develops a probabilistic risk assessment
14 framework to evaluate the wind and rain losses for Australian contemporary houses subjected
15 to non-cyclonic windstorms, which integrates the hazard modelling for extreme wind and
16 associated rainfall, reliability-based wind damage assessment, rainwater intrusion evaluation
17 and economic loss modelling. The risk analysis was conducted for metal-clad contemporary
18 houses in Brisbane and Melbourne. It was found that damage to building interior and contents
19 caused by rainwater intrusion associated with extreme winds is the major contributor to the
20 annual expected economic losses, and houses in Brisbane are generally subjected to higher
21 losses than houses in Melbourne.

22 **Keywords:** Houses; Non-cyclonic windstorms; Wind and rainfall hazard; Economic losses;
23 Probabilistic risk assessment; Rainwater intrusion.

24 *Corresponding author
25
26

27 **1. Introduction**

28 Non-cyclonic windstorms (e.g. synoptic storms associated with low-pressure systems;
29 severe thunderstorms) are the major causes of wind and rainfall damage to housing in Southeast
30 Australia. The three states, Victoria, Queensland and New South Wales, in the southeastern
31 region have more than half of the population of Australia. Loss estimation and risk assessment
32 for housing in these non-cyclonic regions are evidently essential and the key to assessing the
33 cost-effectiveness of relevant wind mitigation measures to reduce the economic losses.

34 Losses and risks to housing during severe windstorms often accrue to damage to the building
35 envelope (Henderson & Ginger 2008; Stewart et al. 2018). The breaches of roof cladding and
36 windows/doors may subsequently induce significant losses to building interior and contents
37 due to rainwater intrusion (e.g. Leitch et al. 2009; Ginger et al. 2010). Qin & Stewart (2019)
38 recently developed a reliability-based fragility method to assess wind-induced roof damage for
39 a representative metal-clad contemporary house in Brisbane and Melbourne. Rainfall often
40 concurs with extreme winds. Subsequent interior and contents losses due to rainwater intrusion
41 through the breaches of building envelope (roof and windows) can now be evaluated based on
42 the wind fragility assessment by Qin & Stewart (2019), where a rainwater intrusion model is
43 proposed herein.

44 The semi-empirical wind-driven-rain (WDR) models (e.g. Straube & Burnett 2000; Blocken
45 & Carmeliet 2004; ISO 2009) have initially been developed for the assessment of moisture,
46 hygrothermal and durability of building facades. The development of the semi-empirical
47 relationships is based on experimental and/or field observations that the amount of WDR
48 depositing on buildings increases approximately proportionally with wind speed and rainfall
49 intensity (Blocken & Carmeliet 2004). Numerical modelling using computational fluid
50 dynamics (CFD) provides an alternative approach for more detailed quantification of WDR
51 (e.g. Choi 1994a; Blocken & Carmeliet 2002). Recently, these WDR methods have been

52 extended to evaluate the amount of rainwater intrusion through building envelope breaches
53 during hurricanes for timber-framed houses in the US (Dao 2010; Dao & van de Lindt 2010;
54 Pita et al. 2012; Baheru et al. 2015; Johnson et al. 2018; Pant & Cha 2019). Although the CFD
55 approach provides a more detailed assessment of WDR, it increases the complexity and cost in
56 both modelling and computation (Blocken & Carmeliet 2010). This may not be suitable for
57 roofs of Australian contemporary houses with large dimensions and complex geometries. The
58 semi-empirical WDR model is thus employed in this study for a convenient and fast evaluation
59 of rainwater intrusion. In this study, the semi-empirical WDR model is modified to suit metal-
60 clad contemporary houses in Australia subjected to non-cyclonic winds. Rainwater intrusion
61 through damaged windows and gaps around undamaged windows that are commonly reported
62 in post-damage investigations (Henderson & Ginger 2008; Ginger et al. 2010; Henderson et al.
63 2017) is also considered in this study.

64 The loss estimation and risk assessment for houses in the US are based on existing wind and
65 rainfall models for hurricanes (e.g. Pita et al. 2012; Johnson et al. 2018; Pant & Cha 2019).
66 However, there is a lack of hazard models for rainfall associated with non-cyclonic extreme
67 winds. Thus, this study newly develops a probabilistic model to characterize the duration and
68 the average rainfall intensity for non-cyclonic windstorms using regional wind and rainfall data
69 of Brisbane and Melbourne. This model can be used for the subsequent rainwater intrusion
70 assessment after wind damage. Loss estimation is conducted based on cost data obtained from
71 Australian housing cost guides (Rawlinsons 2015). The loss functions is dependent on the
72 extent of wind damage to housing components and the volume of rainwater intrusion yielded
73 by the wind fragility analysis and the rainwater intrusion model, respectively, and are
74 developed according to the loss modelling in HAZUS (2014) and engineering judgement. By
75 integrating the hazard model for extreme wind and associated rainfall, wind damage and
76 rainwater intrusion assessment, and loss modelling, this study conducts a probabilistic risk

77 assessment for the representative contemporary house in Brisbane and Melbourne. The
78 obtained annual expected economic losses can further facilitate the risk mitigation and climate
79 adaptation for housing in non-cyclonic regions of Australia.

80 **2. Risk Assessment Framework**

81 The risk from extreme winds is expressed as (Stewart et al. 2018)

$$82 \quad E(L) = \sum \Pr(H) \Pr(DS|H) \Pr(L|DS) L \quad (1)$$

83 where $\Pr(H)$ is the probability of a wind hazard. The wind hazard is typically represented by
84 the wind speed, which can be further extended to include other environmental hazard of interest
85 (e.g. rainfall, windborne debris, storm surge) commonly associated with or induced by the
86 extreme wind event. $\Pr(DS|H)$ is the probability of a damage state conditional on the hazard
87 (fragility), $\Pr(L|DS)$ is the conditional probability of a loss given occurrence of the damage,
88 and L is the loss or consequence if full damage occurs. According to post-damage surveys (e.g.
89 Leitch et al. 2009), the majority of losses to contemporary houses result from wind damage to
90 roof and fenestrations (especially windows), and the subsequent rainwater damage to building
91 interior and contents. Wind-induced damage to other housing components (e.g. walls) is rare
92 for contemporary houses in non-cyclonic regions of Australia. Therefore, the possible losses
93 considered in this study arise from wind damage to metal roof cladding and timber roof framing,
94 windward windows, and rainwater damage to building interior and contents as well as the loss
95 of use.

96 **3. Hazard Modelling**

97 **3.1. Extreme wind speed**

98 The peak gust wind speed in non-cyclonic regions of Australia, v (m/s), is modelled by a
99 Gumbel distribution. The cumulative distribution function (CDF) for annual maximum gust
100 wind speed is given by (Wang et al. 2013; Stewart et al. 2018)

$$101 \quad F_V(v) = e^{-e^{-\frac{v-v_g}{\sigma_g}}} \quad (2)$$

102 where v_g and σ_g are the location and scale parameter, respectively. The gust wind speed v is the
 103 maximum 0.2 second gust velocity at 10 m height in open terrain. Figure 1 depicts the extreme
 104 gust wind speed corresponding to various return periods. The location and scale parameters are
 105 given as $v_g=26.0326$, $\sigma_g=4.0488$ for Brisbane and $v_g=27.7777$, $\sigma_g=1.664$ for Melbourne (Wang
 106 et al. 2013; Stewart et al. 2018).

107 **3.2. Rainfall associated with extreme winds**

108 An extreme wind event is often associated with rainfall. When assessing rainwater intrusion
 109 and the consequent damage to building interior and contents, it is ideal to have the joint
 110 probability of wind speed and rainfall intensity rather than treating these two weather variables
 111 independently. In addition, the average rainfall intensity (R_h) during a windstorm is typically
 112 dependent on the duration, e.g. intense burst of rainfall is more likely to occur in a short event.

113 The exponential distribution is connected to the Poisson arrival process, and commonly used
 114 to model the storm duration (e.g. Eagleson 1972; Koutsoyiannis & Georgiou 1993; Lambert &
 115 Kuczera 1998). A two-parameter exponential distribution is adopted in this study to model the
 116 windstorm duration (D_{ur}) with the CDF given by

$$117 \quad F(D_{ur}) = 1 - e^{-\lambda(D_{ur}-\mu)} \quad (3)$$

118 where λ and μ are the rate and location parameter, respectively.

119 A gamma distribution is used to model the average rainfall intensity during an extreme
 120 windstorm. The probability density function (PDF) of the gamma distribution is given by

$$121 \quad g(R_h) = \frac{R_h^{\gamma-1} e^{-\frac{R_h}{\beta(D_{ur})}}}{\Gamma[\gamma]\beta(D_{ur})^\gamma} \quad (4)$$

122 where $\Gamma(\cdot)$ is the gamma function, γ is the shape parameter, and $\beta(D_{ur}) = a_0 + a_1(1/D_{ur})$ is the
 123 scale parameter which is assumed to have a linear relationship with the reciprocal of D_{ur} . Note

124 that R_h in Eq. (4) is greater than zero, and hence the gamma distribution is only used when
125 rainfall occurs simultaneously with strong winds. Accounting for the probability of no rain (P_{no})
126 during a windstorm, the CDF of R_h ($R_h \geq 0$) is given by

$$127 \quad F(R_h) = P_{no} + (1 - P_{no})G(R_h) \quad (5)$$

128 where $G(R_h)$ is the CDF of the gamma distribution given by Eq. (4) to model the non-zero R_h ,
129 and P_{no} can be estimated from the meteorological data.

130 The model parameters of the exponential and gamma distribution are estimated using the
131 meteorological data from two weather stations, i.e. Archerfield airport in Brisbane and
132 Moorabbin airport in Melbourne. A twenty-year length of half hourly wind and rainfall data
133 from 1996 to 2015 for these two weather stations are obtained from the Australian Bureau of
134 Meteorology (BoM). A windstorm with the maximum gust wind speed greater than 36 knots
135 (i.e. 18.5 m/s or 66.7 km/hr) is considered as an extreme wind as strong wind warnings can be
136 issued at this wind speed by BoM. A total of 86 and 364 severe windstorms from 1996 to 2015
137 are then extracted from the meteorological data for Archerfield and Moorabbin airports,
138 respectively, and for each storm event, the duration and average rainfall intensity (accumulative
139 rainfall depth divided by storm duration) are obtained. The number of storm events with no
140 rain (i.e. $R_h = 0$) is also obtained to estimate P_{no} .

141 Figure 2 shows the exponential probability plots for D_{ur} , which suggests that the two-
142 parameter exponential distribution given by Eq. (3) fits well to the storm duration data. It is
143 estimated that $P_{no} = 25.6\%$ and 45.9% for Brisbane and Melbourne, respectively. The model
144 parameters in the gamma regression formulation given by Eq. (4) are estimated using the
145 generalized linear model in the R software package (R Core Team 2019). Figure 3 shows the
146 mean and quantile values produced by the gamma model as a function of D_{ur} . The average
147 rainfall intensity data is also plotted in the same figure, which indicates that Brisbane tends to
148 have shorter windstorms with more intense rainfall (e.g. thunderstorms), whereas windstorms

149 in Melbourne are generally longer with lower average rainfall intensity. Figure 3 suggests a
150 good predictability of the gamma model to capture the average rainfall intensity during
151 windstorms. Note that the estimated model parameters for D_{ur} and R_h can only be rigorously
152 applied to the risk assessment for houses in the surrounding or nearby suburbs of Archerfield
153 airport and Moorabbin airport, however it can be further extended to incorporate more weather
154 stations in Brisbane and Melbourne, and account for the spatial variations and patterns of
155 rainfall. Other probability distributions, e.g. Weibull, lognormal, Generalized Pareto, have also
156 been reported in the literature to model the rainfall intensity (e.g. Heneker et al. 2001;
157 Koutsoyiannis et al. 2003; Mudd et al. 2016), however, it is out of the scope of this study to
158 examine which is the best fit to the local meteorological data. The accuracy of estimation can
159 be further improved by incorporating more years of data, if available.

160 **4. Wind Damage**

161 **4.1. Roof fragility**

162 A reliability-based fragility method has been developed by Qin & Stewart (2019) to assess
163 the wind damage to metal roof cladding and timber roof trusses for Australian contemporary
164 houses. The fragility analysis was conducted for a representative contemporary house in the
165 Australian suburbs of Brisbane and Melbourne. The house has a complex hip roof and is a
166 wood-frame brick-veneer construction with a roof slope of 21.5° . Windows are generally
167 sliding or awning windows with a brick on edge or terracotta tiled window sill. Corrugated
168 metal roof sheets are installed and connected to metal top-hat battens. Figure 4 depicts the 3D
169 and plan view of the representative one-storey house. See Parackal et al. (2016) for more
170 details.

171 The fragility of the roof system is defined as the extent of roof sheeting loss and roof truss
172 failures at a given gust wind speed. The overloading of cladding-to-batten (CTB), batten-to-
173 rafter/truss (BTR) and rafter/truss-to-wall (RTW) connections is considered to cause the failure

174 of metal roof sheeting and timber roof trusses as these roof connections are generally the
175 ‘weakest links’ of the roof system (Henderson & Ginger 2007). The limit state function for a
176 single roof connection is

$$177 \quad g = R - (W - D_L) \quad (6)$$

178 where R is the connection resistance, W is the wind uplift loads acting on this connection, and
179 D_L is the dead load accounting for the weight of roof components. A connection is deemed to
180 fail if $g \leq 0$. The probabilistic models for the wind loading and connection resistances are given
181 by Qin & Stewart (2019). The uplift forces in roof connections are obtained using a FE
182 approach described in Qin & Stewart (2019).

183 In the fragility analysis, two typical scenarios are assumed for the internal pressurization,
184 i.e. (i) the existence of windward dominant openings, and (ii) without any wall openings. A
185 Monte Carlo Simulation (MCS) analysis in conjunction with the FE approach are employed to
186 assess the wind fragility for roof cladding and trusses, which enables the probabilistic
187 characterization of spatially varying wind uplift pressures, uplift forces in roof connections,
188 progressive failure and load redistribution after initial local damage, and internal pressure
189 changes with increasing sheeting loss. A total of 1,646 CTB, 532 BTR and 38 RTW
190 connections are involved in the MCS analysis and FE approach. The fragility curves yielded
191 by the MCS and FE approach express the extent of roof sheeting loss (R_{clad}) and the proportion
192 of roof truss failures (R_{truss}) as a function of gust wind speed. According to AS4055 (2012),
193 suburban houses in Brisbane generally have design wind classifications of N2 and N3, and
194 those in Melbourne are typically with design wind classifications of N1 and N2. The mean
195 proportions of roof sheeting loss and roof truss failures produced by the fragility assessment
196 are shown in Fig. 5. The RTW connectors are different for houses with design wind
197 classifications of N1, N2 and N3. Note that the fragility results apply to suburban houses (i.e.
198 the nominal value for terrain and height factor is 0.83 as given by AS/NZS 1170.2 2011) on a

199 flat site without shielding and wind directionality effects but have the flexibility to account for
200 other site conditions. Refer to Qin & Stewart (2019) for more details about the fragility analysis.

201 **4.2. Window damage**

202 The windward dominant openings and associated rainwater intrusion are considered to
203 result from the breakage of windows by high wind pressure. The wind pressure acting on the
204 windward window (W_{win}) is calculated based on the gust wind speed and the wind loading
205 parameters (e.g. terrain and height factor, shielding factor, wind directionality factor, pressure
206 coefficients, etc.). An external wall pressure coefficient is assumed to follow a normal
207 distribution with a mean of 0.70 and a coefficient of variation (COV) of 0.15 (Henderson &
208 Ginger 2007). The internal pressure coefficient is calculated based on the approach given by
209 Qin & Stewart (2019) considering the failure progression of metal roof sheets. Note that
210 window failure caused by windborne debris is not considered in this study because the damage
211 assessment is only conducted for a single house instead of a residential community where
212 debris are often generated from neighbourhood houses. In addition, windborne debris is less of
213 a concern in non-cyclonic regions of Australia as indicated in AS/NZS 1170.2 (2011).

214 According to AS2047 (2014), windows shall not fail when tested under the ultimate limit
215 state pressure, and shall not have penetration of uncontrolled water when tested under the water
216 penetration resistance test pressure. The ultimate strength (R_{ult}) and water penetration resistance
217 (R_{water}) of windows are assumed to follow a normal distribution (HAZUS 2014). It is further
218 assumed that the COV is 0.20 and that 20% of the windows do not satisfy the test pressures
219 specified in AS2047 (2014) to account for the variance of quality in manufacture and
220 installation (HAZUS 2014). In other words, the mean ultimate strength and water penetration
221 resistance are about 1.20 times the test pressures specified in AS2047 (2014). The statistics for
222 window resistances are given in Table 1, and the limit states used for windward windows are
223 shown in Table 2.

224 **5. Rainwater Intrusion**

225 The quantification of rainwater intrusion is also conducted under two wall opening scenarios:

226 (i) with windward dominant openings (with window breakage) and (ii) without any wall
227 openings (without window breakage). For the dominant opening scenario, the main source of
228 rainwater intrusion considered is water entering from roof and window breaches. Due to high
229 wind pressures acting on the windward wall during an extreme wind event, water entry through
230 undamaged windows has been commonly reported in post-damage surveys (Henderson &
231 Ginger 2008; Ginger et al. 2010). This is likely because the high differential pressures across
232 windows exceed the water penetration resistances of windows. For the scenario without any
233 wall openings, rainwater is thus considered to enter through roof breaches and gaps around
234 windward windows. The rainwater intrusion via any gaps and cracks on undamaged roof
235 cladding is neglected because the metal roof is mostly subjected to suction pressures, and is
236 generally more watertight.

237 Given the occurrence of strong wind, the rain is endorsed a horizontal velocity by the wind
238 and then falls obliquely. The vertical component of the oblique rainfall passing through a
239 horizontal plane is typically measured at the meteorological stations, while the horizontal
240 component passing through a vertical plane, defined as wind-driving rain (WDR), is not
241 measured and needs to be quantified by relevant WDR methods. A semi-empirical WDR model
242 (e.g. Straube & Burnett 2000; Blocken & Carmeliet 2004; ISO 2009) is employed in this study
243 to assess the amount of driving rain entering the breaches and gaps in the building envelope.
244 An empirical runoff model is also applied to assess the water ingress due to rainwater runoff
245 from upstream undamaged building envelope.

246 **5.1. Free-field WDR intensity**

247 It is assumed that the wind flow is uniform, steady and horizontal, and the horizontal
248 velocity of the raindrops is equal to the wind speed. Then the free-field WDR intensity

249 (unobstructed by the building), R_{WDR} (mm/hour), passing through an imaginary vertical plane
250 is given by (Straube & Burnett 2000; Blocken & Carmeliet 2004)

$$251 \quad R_{WDR} = DRF \cdot R_h \cdot U \quad (7)$$

252 where U (m/s) is the mean wind speed, R_h (mm/hr) is the average rainfall intensity, $DRF = 1/V_t$
253 is the driving rain factor, and V_t (m/s) is the terminal velocity of raindrops (i.e. vertical falling
254 speed of raindrops). The driving rain factor DRF is a function of the rainfall intensity R_h , and
255 is evaluated using the approach given by Choi (1994b). Table 3 shows the DRF values
256 corresponding to various rainfall intensities.

257 The mean wind speed, U , can be linked to the maximum gust wind speed, v , by the following
258 equation

$$259 \quad U = (E \cdot D \cdot T) \cdot v / G_u \quad (8)$$

260 where E is the terrain height factor to model the exposure and building height, D is a factor for
261 wind directionality effects, T is the shielding factor, and G_u is the velocity gust factor used to
262 approximately convert a peak gust wind speed to corresponding mean wind speed. The factors
263 E , D and T are assumed to follow a lognormal distribution with the mean-to-nominal ratios and
264 COV values given in Qin & Stewart (2019). The corresponding nominal values of these factors
265 can be obtained from AS/NZS 1170.2 (2011) for different site conditions. For an hourly mean
266 wind speed, a gust duration of 0.2s and a turbulence intensity of 0.20 (open terrain), a value of
267 1.77 is calculated for G_u (ESDU 2002). Table 4 shows the G_u values corresponding to different
268 averaging periods calculated according to ESDU (2002).

269 **5.2. Driving rain intrusion**

270 5.2.1. Roof breaches

271 The volumetric rate of oblique driving rain intrusion (litre/hr) via a roof opening is

$$272 \quad VOL_R = RAF_R \cdot R_{WDR} \cdot A_{SV} \quad (9)$$

273 where RAF_R is the rain admittance factor (Straube & Burnett 2000) for roof which is the ratio
274 of the rainwater intrusion intensity to the free-field WDR intensity, R_{WDR} is the free-field WDR
275 intensity given by Eq. (7), A_{SV} is the vertical projection area of a metal roof sheet opening with
276 $A_{SV} = A_S \sin(\alpha)$, where A_S is the area of the damaged metal sheet and α is the roof slope (21.5°
277 for the representative contemporary house). The RAF_R mainly depends on building geometries
278 and aerodynamics to account for the building disturbance to the free-field WDR.

279 The RAF_R value is estimated based on limited experimental evidence (Baheru et al. 2014).
280 The RAF_R for roof openings on the windward side is assumed to follow a truncated normal
281 distribution with a mean of 0.30 and a standard deviation of 0.20 (truncated to an interval of 0
282 to 1), whereas the RAF_R value for roof openings on the leeward side is zero. For roof openings
283 parallel to the wind direction, the RAF_R is assumed to follow a truncated normal distribution
284 with a mean of 0.05 and a standard deviation of 0.05 (truncated to an interval of 0 to 1). For
285 oblique wind angles, it can be approximately accounted for by projecting onto directions
286 normal and parallel to the building facades (Straube & Burnett 2000; Blocken & Carmeliet
287 2004). As the building geometries and wind conditions in Baheru et al. (2014) do not exactly
288 match those for the representative house examined in this study, a relatively large standard
289 deviation is selected for the truncated normal distribution of RAF_R values to implicitly account
290 for the uncertainties involved. The statistical parameters for RAF_R are summarized in Table 5.
291 There is a clear need to modify the estimation of RAF_R values with more evidence from
292 experiments and/or CFD studies to better inform the semi-empirical model, and hence improve
293 the accuracy of the rainwater intrusion model.

294 5.2.2. Window breaches

295 Only the horizontal component of the oblique driving rain enters window breaches. The
296 volumetric rate of driving rain intrusion via a window opening is

$$297 \quad VOL_W = RAF_W \cdot R_{WDR} \cdot A_W \quad (10)$$

298 where A_W is the area of the window opening, and RAF_W is the rain admittance factor for
299 window. The value of RAF_W is only non-zero for window openings on the windward wall,
300 which is assumed to follow a truncated normal distribution with a mean of 0.50 and a standard
301 deviation of 0.20 (truncated to an interval of 0 to 1) as inferred from Straube & Burnett (2000)
302 and Baheru et al. (2014) as shown in Table 5. A cosine projection (Straube & Burnett 2000;
303 Blocken & Carmeliet 2004) can be used to approximately account for the rain driven by oblique
304 wind (i.e. wind angle is non-normal to the wall/window).

305 5.2.3. Gaps around windows

306 The volumetric rate of driving rain intrusion via gaps around the window is given by

$$307 \quad VOL_G = f_v \cdot RAF_W \cdot R_{WDR} \cdot A_G \quad (11)$$

308 where A_G is the area of the gap (mm^2), and f_v is a velocity ratio that accounts for the speed
309 change of air as it passes through small gaps, cracks and openings on buildings (Baheru et al.
310 2015). As shown in Table 5, the f_v value is assumed to follow a normal distribution with a mean
311 of 2.50 and a standard deviation of 0.30 which is estimated based on the environmental design
312 guide CIBSE (2015) for air infiltration driven by wind through small gaps in buildings. A gap
313 width of 0.5 mm is assumed for windows in the representative contemporary house.

314 5.3. Rainwater runoff

315 The rainwater runoff is another source of rainwater intrusion through breaches and gaps in
316 the building envelope. A portion of the oblique driving rain deposited on the upstream
317 undamaged building envelope can run into the damaged roof sheets and windows. The
318 volumetric rate of rainwater runoff into a roof or window opening (VOL_{RO}) is simply calculated
319 by applying a reduction factor, f_r , to the volumetric rate of driving rain impinging on the
320 upstream surface of undamaged building envelope. For example, Fig. 6 shows the upstream
321 runoff surface of a roof opening. This reduction factor accounts for the loss of rainwater amount
322 due to splashing, evaporation, absorption and adhesion, which is assumed to follow a truncated

323 normal distribution with a mean of 0.25 and a standard deviation of 0.15 (truncated to an
324 interval of 0 to 1) as shown in Table 5. This estimation is based on the engineering judgement
325 that the representative contemporary house only experiences a small portion of runoff water.
326 The basis of this engineering judgement are given herein. A brick veneer wall has great capacity
327 for water absorption to reduce rainwater runoff through windows. Windows on Australian
328 contemporary houses are typically positioned very close to the eave with limited area of
329 upstream surface for rainwater runoff. The corrugation of metal roof sheets reduces rainwater
330 runoff through roof openings. Sensitivity analyses for the factors listed in Table 5 are conducted
331 in Section 7.2.3 to examine their effects on the risk assessment.

332 **5.4. Volumetric rate of rainwater intrusion**

333 A MCS analysis is employed to evaluate the total volumetric rate of rainwater intrusion
334 VOL_T (litre/hr) through roof and window breaches, and gaps around the window (i.e. VOL_R ,
335 VOL_W , VOL_G , and VOL_{RO} for all building envelope breaches and gaps). For the dominant
336 opening scenario, the total size of openings due to window breakage on a windward wall is
337 estimated to be 4m^2 . A sensitivity analysis is conducted in Section 7.2.3 for a different opening
338 size. The MCS used for wind fragility analysis is extended to assess the subsequent rainwater
339 intrusion by applying the semi-empirical model. The volumetric rates of rainwater intrusion
340 are dependent on the number and locations of failed roof sheets obtained from the fragility
341 analysis, and also a function of gust wind speed and rainfall intensity.

342 Figure 7 shows the mean VOL_T for the two wall opening scenarios. As expected, the mean
343 VOL_T increases with wind speed and rainfall intensity. The nonlinearity of rainwater intrusion
344 with increasing wind speed is because there is more roof sheeting loss at a higher wind speed
345 allowing for more rainwater intrusion. Figure 8 shows the mean volumetric rates of rainwater
346 intrusion through roof and window, respectively, under the two wall opening scenarios at a
347 rainfall intensity of 10 mm/hr, which suggests that the rainwater intrusion via window is higher

348 than that through roof openings for relatively lower wind speeds. With an increasing wind
349 speed, more roof openings tend to occur due to increasing metal roof sheeting loss, which
350 results in more rainwater intrusion via roof openings.

351 **5.5. Volume of rainwater intrusion**

352 The evolution of internal pressurisation and load redistribution due to the progressive failure
353 of the building envelope are explicitly accounted for in the wind damage assessment (see Qin
354 & Stewart 2019 for more details), however, the temporal damage progression of the building
355 envelope is not explicitly considered. It is assumed that the roof damage and the exceedance of
356 limit states for windward windows given by Table 2 all happen at the occurrence time of the
357 maximum gust wind speed (T_M) during a windstorm. The volume of rainwater intrusion (VOL)
358 through all breaches and gaps in the building envelope is then given by

$$359 \quad VOL = VOL_T \cdot T_R \quad (12)$$

360 where $T_R = D_{ur} - T_M$ is the length of time after the wind damage to the building envelope, and
361 T_M is assumed to follow a uniform distribution with a lower bound of zero and an upper bound
362 of D_{ur} . Note that VOL_T evaluated in Section 5.4 is based on the average rainfall intensity R_h .
363 This is another approximation that the temporal variation of rainfall intensity during a
364 windstorm is not explicitly taken into account, and hence the assessment of rainwater intrusion
365 volume in this study is not fully event-based.

366 **6. Loss Modelling**

367 **6.1. Subassembly cost ratios**

368 The loss estimation uses an assembly-based approach (e.g. Porter et al. 2001; HAZUS 2014;
369 Hamid et al. 2010; Stewart et al. 2018). The entire house is divided into subassemblies/
370 components based on specific building details. Then the total loss is equal to the sum of repair
371 or replacement costs of every housing components. The loss estimation takes into account
372 housing components/subassemblies that are related to the failure of roof cladding and trusses,

373 windward windows, and those susceptible to rainwater damage. The representative
 374 contemporary house described in Section 4.1 is then divided into subassemblies as shown in
 375 Table 6. The subassemblies (e.g. site preparations, foundations, wall structures, etc.) that are
 376 not explicitly included in the loss estimation are categorized under ‘other’.

377 The losses are estimated in terms of cost ratios. Herein, the cost ratio of a subassembly is
 378 defined as the ratio of the cost to complete the subassembly (i.e. newly build, upgrade, repair
 379 or replace) to the building value. The estimated total cost to build a new contemporary house
 380 with an approximate floor area of 150 m² is $L_{building} = \$300,000$ Australian Dollars (HIA 2018
 381 and RLB 2019). Based on cost data provided by Australian housing cost guides (Rawlinsons
 382 2015) and subjective judgement, the subassembly cost ratios are estimated for a representative
 383 contemporary house built to an average standard as shown in Table 6. Note that the cost ratios
 384 in Table 6 are estimated for new construction that includes material and labour costs plus
 385 contractor’s overhead and profit. In the context of this study, cost ratios for repair and/or
 386 replacement of damaged components/subassemblies are needed, which can be obtained by
 387 adjusting the cost ratios in Table 6 using a factor of 1.25 to account for the additional costs
 388 associated with removal, repair and remodelling of an existing house (HAZUS 2014), and a
 389 factor of 1.05 to account for increased contractor’s overhead and profit for repair and/or
 390 replacement work (Rawlinsons 2015). The adjusted cost ratios are also given in Table 6.

391 **6.2. Loss functions**

392 6.2.1. Roof cladding loss

393 Insurance data in Australia suggests that the metal roof is likely to be entirely replaced if the
 394 proportion of roof sheeting damage exceeds 20% (Smith & Henderson 2015), hence,

$$395 \Pr(L_1 | DS = R_{clad}) = \begin{cases} R_{clad} & R_{clad} \leq 20\% \\ 1.0 & R_{clad} > 20\% \end{cases} \quad (13)$$

396 where R_{clad} is the proportion of metal roof cladding damage and $L_1 = 5.4\%$ is the cost ratio for

397 full replacement of roof cladding.

398 6.2.2. Roof framing loss

399 The cost ratio for a full roof framing replacement is $L_2 = 20.9\%$. The roof framing includes
400 timber roof trusses, jack and hip rafters, ridgeboard, valley rafters, struts and ties, ceiling joists,
401 fixings and connections, etc. In the wind fragility assessment, only the failures of critical roof
402 trusses are explicitly evaluated. It is assumed that the failure of a critical truss causes damage
403 to other framing elements directly and/or indirectly linked to this truss. In this study, a threshold
404 value of 20% is assumed for a full replacement of the roof framing based on existing loss
405 functions and damage states used in the literature (e.g. van de Lindt & Dao 2012; Li et al. 2011).
406 In other words, if the damage proportion of the critical roof trusses exceeds this threshold value,
407 a full replacement of the entire roof framing is then required, leading to

$$408 \Pr(L_2|DS = R_{truss}) = \begin{cases} R_{truss} & R_{truss} \leq 20\% \\ 1.0 & R_{truss} > 20\% \end{cases} \quad (14)$$

409 where R_{truss} is the damage proportion of the critical roof trusses.

410 6.2.3. Windward windows

411 The ratio of windward window loss caused by high wind pressure is expressed as

$$412 \Pr(L_3|DS) = \begin{cases} 0 & W_{win} < R_{ult} \\ 1.0 & W_{win} \geq R_{ult} \end{cases} \quad (15)$$

413 where $L_3 = 1.0\%$.

414 6.2.4. Interior loss

415 The building interior considered in the loss estimation includes internal finishes and fittings,
416 mechanical and electrical systems. The cost ratio for a full replacement of interior is $L_4 = 51.2\%$.
417 The interior loss is modelled as a function of rainwater intrusion, and it is assumed that the
418 interior losses increase linearly with an increasing amount of rainwater intrusion until

419 exceeding a threshold value to cause a complete loss (Pita et al. 2012; HAZUS 2014). The
 420 proportion of interior loss due to rainwater damage is

$$421 \quad \Pr(L_4|DS = h_I) = \begin{cases} \frac{h_I}{h_T} & h_I \leq h_T \\ 1.0 & h_I > h_T \end{cases} \quad (16)$$

422 where h_I (mm) is the accumulated water depth calculated as the total rainwater intrusion volume
 423 VOL given by Eq. (12) divided by the floor area of the entire house, and h_T (mm) is a threshold
 424 value of water depth that leads to total interior loss. A threshold value of $h_T = 25$ mm given by
 425 Pita et al. (2012) is used in this study. A sensitivity analysis for h_T is presented in Section 7.2.3
 426 to examine its effect on annual expected losses.

427 6.2.5. Contents loss

428 The contents loss is also modelled as a function of rainwater intrusion. The contents loss is
 429 directly related to rainwater entering from windows, and it is assumed that the contents can
 430 only be damaged by rainwater entering from the roof if the ceiling leaks (e.g. due to local
 431 damage of a ceiling). In this case, a weighting factor, $w_0 = 0.6$, is assumed for the proportion of
 432 water depth resulting from a damaged roof that causes contents loss. A sensitivity analysis is
 433 conducted in Section 7.2.3 for this weighting factor. Using the same threshold value of water
 434 depth, $h_T = 25$ mm, the proportion of contents loss due to rainwater damage is

$$435 \quad \Pr(L_5|DS = w_0 h_R + h_W) = \begin{cases} \frac{w_0 h_R + h_W}{h_T} & w_0 h_R + h_W \leq h_T \\ 1.0 & w_0 h_R + h_W > h_T \end{cases} \quad (17)$$

436 where h_R and h_W are the accumulated water depth due to rainwater intrusion via roof and
 437 windows, respectively. Based on the statistics of the average value of a household's home
 438 contents in Australia (ABS 2011), it is estimated that $L_5 = 25.0\%$.

439 6.2.6. Loss of use

440 The annual probability of loss of use due to housing damage is (HAZUS 2014)

$$441 \quad \Pr(L_6|DS) = \frac{N_{\text{Iou}}(\Pr(L_{\text{building}}|DS) L_{\text{building}}) \cdot \text{Mod}(\Pr(L_{\text{building}}|DS) L_{\text{building}})}{365} \quad (18)$$

442 where N_{Iou} is the loss of use (days) accounting for delays in decision-making, financing,
 443 inspection, etc., and Mod is a multiplier to account for the fact that the house can still be
 444 occupied if damage is not severe (HAZUS 2014). Both N_{Iou} and Mod are modelled as a function
 445 of the expected total building loss, i.e. $\Pr(L_{\text{building}}|DS)L_{\text{building}}$, which is a summation of all the
 446 subassembly losses (excluding contents loss) considered in this study (i.e. $\sum_{i=1}^4 \Pr(L_i|DS) L_i$).
 447 Detailed values for N_{Iou} and Mod can be found in HAZUS (2014) and Stewart et al. (2018).
 448 The annual loss of use (365 days) corresponds to a cost ratio of $L_6 = 16.3\%$ based on an
 449 estimated additional living cost of \$1,000 per week (e.g. rent, hotel costs, relocation and
 450 increased transportation fees, furniture rental costs, etc.).

451 **7. Economic Losses and Risks**

452 **7.1. Risk analysis method**

453 The annual risk (expressed as the expected loss) is given by

$$454 \quad E_{\text{annual}}(L) = \int_0^{\infty} \int_0^{\infty} \int_0^{\infty} f(R_h | v, D_{ur}) f(v) f(D_{ur}) \frac{1}{n_d} \sum_{j=1}^{n_d} \left[\Pr(DS | D_{Nj} T_N v, R_h, D_{ur}) \sum_{i=1}^{n_c} \Pr(L_i | DS) L_i \right] dv dR_h dD_{ur} \quad (19)$$

455 where $f(v)$ is the probability distribution of the annual maximum gust wind speed, $f(R_h | v, D_{ur})$
 456 is the probability distribution of the average rainfall intensity of a severe windstorm
 457 corresponding to a given duration D_{ur} , $f(D_{ur})$ is the probabilistic distribution of the windstorm
 458 duration, $n_d = 8$ is the number of cardinal wind directions considered in this study, $n_c = 6$ is the
 459 number of subassemblies/components considered in the loss estimation as described in Section
 460 6, D_N is the nominal wind directionality factor for eight cardinal directions, and T_N is the
 461 nominal value of the shielding factor, $\Pr(DS | v, R_h, D_{ur})$ is the likelihood of damage state (e.g.
 462 extent of roof damage, amount of rainwater intrusion) given the gust wind speed, rainfall
 463 intensity and storm duration, $\Pr(L_i | DS)$ is the loss likelihood for the i^{th} component/subassembly

464 described in Section 6.2, and L_i is the maximum probable loss for the i^{th}
465 subassembly/component.

466 The probabilistic models for $f(v)$, $f(D_{ur})$ and $f(R_h | v, D_{ur})$ are described in Section 3. The D_N
467 and T_N values are obtained from AS/NZS 1170.2 (2011) for suburban houses in Brisbane and
468 Melbourne with different site conditions and design wind classifications (see Table 7). Note
469 that Eq. (19) assumes that damage is caused by the largest windstorm in any calendar year,
470 which slightly underestimates the risks due to the ignorance of less severe windstorms in the
471 same year. An alternative way is the adoption of a Poisson distribution to model the number of
472 severe windstorms in a calendar year, and a Generalized Pareto distribution for the maximum
473 gust wind speed in each windstorm (i.e. method of ‘peaks over threshold’). This is subjected to
474 further examination if more meteorological data are accessible.

475 The probabilistic risk assessment conducted using a MCS analysis consists of four major
476 components, i.e. (i) hazard modelling for wind and rainfall, (ii) reliability-based wind damage
477 assessment, (iii) evaluation of rainwater intrusion, and (iv) loss estimation. Figure 9 shows an
478 outline to illustrate the risk analysis method to assess the annual expected economic losses for
479 the representative contemporary house subjected to non-cyclonic extreme winds and associated
480 rainfall.

481 **7.2. Results**

482 The risk analysis is conducted for the representative contemporary house built in suburbs of
483 Brisbane and Melbourne. The CTB and BTR connections are considered to be identical for
484 houses with different design wind classifications, whereas the RTW connections and window
485 strengths are different. The higher the design wind classification, the stronger the RTW
486 connections and windows (i.e. with higher ultimate strength against wind pressure). However,
487 this is not the case for the water penetration resistance of windows (see Table 1).

488 7.2.1. Annual expected losses

489 Table 8 shows the total annual expected losses (normalized by the building value) including
490 the loss of use (i.e. L_6). The annual expected losses to each housing component/subassembly
491 (L_1 to L_5 described in Section 6.2), the average days for loss of use in a calendar year and the
492 proportion of window breakage (i.e. dominant opening scenario) are also given in Table 8. As
493 shown in this table, building interior and contents losses are the major contributor to the annual
494 risks (i.e. more than 90% of the total building loss), which is much larger than the direct losses
495 to metal roof cladding, timber roof framing and windward windows. This is because the annual
496 expected damage proportions of roof and windows are small. In addition, the costs to repair or
497 replace roof and windows are much less than those for building interior and contents. Although
498 the economic losses directly caused by roof sheeting loss and window breakage are not
499 significant, a small portion of such building envelope breaches may induce significant losses
500 to building interior and contents due to rainwater intrusion.

501 As indicated in Table 8, window breakage is rare, and hence the non-dominant opening
502 scenario is more likely to occur. Since the proportion of roof sheeting loss is small under the
503 non-dominant opening scenario as shown in Fig. 5(a), in most cases, more rainwater enters
504 through gaps around windward windows when the water penetration resistance is exceeded
505 (see Fig. 8). For example, the Brisbane house with a wind classification of N2 suffers more
506 losses from rainwater intrusion than the house with a wind classification of N3, mainly due to
507 a lower water penetration resistance of the windward wall window (see Table 1). Melbourne
508 houses with a design wind classification of N2 are subjected to higher wind pressure than those
509 with a design wind classification of N1 but the water penetration resistances of the windward
510 window are comparable. This results in slightly higher building interior and contents losses for
511 Melbourne houses with a design wind classification of N2. Table 8 also indicates that houses
512 in Brisbane are generally subjected to higher losses than houses in Melbourne because the

513 extreme wind speed and rainfall intensity are higher in Brisbane, though Brisbane houses have
514 been designed to resist higher wind speed. Note that the annual risks presented in Table 8 may
515 be used as a lower bound. Construction defects are common in housing construction, which
516 can increase the roof damage and also subsequently incur more rainwater damage.
517 Incorporation of the construction defects in the risk analysis will be conducted in a future study.
518 Moreover, window breakage by windborne debris can be further incorporated if a residential
519 community is considered.

520 Table 9 shows the mean proportions of wind damage to metal roof cladding and timber roof
521 trusses, and the mean depth of rainwater intrusion at the 50-year and 500-year gust wind speed
522 (i.e. V_{50} and V_{500}). Table 9 suggests that the metal roof cladding and timber roof trusses are
523 subjected to negligible damage at the 50-year wind speed, which is expected. At the wind speed
524 $V_{50} = 35$ m/s for Melbourne and $V_{50} = 43$ m/s for Brisbane, houses are more likely under the
525 non-dominant opening scenario, and the proportions of roof sheeting loss and roof truss failures
526 are close to zero (see Fig. 5). The losses at V_{50} are mainly due to the rainwater intrusion through
527 gaps around windward windows. At the 500-year wind speed, Brisbane houses with a design
528 wind classification of N2 are subjected to more damage to roof trusses than those with a design
529 wind classification of N3, because the former has weaker RTW connections (see Fig. 5b).
530 Slight roof truss damage is predicted for Melbourne houses at V_{500} . The amount of rainwater
531 intrusion increases at V_{500} due to the increasing building envelope breaches and wind speed.

532 7.2.2. Implications for insurance premium

533 According to Goda & Hong (2008), the annual insurance premium (INP) charged by an
534 insurer for a building is

$$535 \quad INP = (1 + \eta) \cdot E[I(ML)] \quad (20)$$

536 where $E[I(ML)]$ is the annual expected value of indemnity $I(ML)$, and η is the insurance loading
537 factor. As inferred from Walker et al. (2016), η is typically greater than 0.3 to account for

538 administration costs and profits, and could be considerably large for high exposure areas. The
 539 indemnity $I(ML)$ is expressed as a function of the monetary loss ML (Goda & Hong 2008),
 540 given by

$$541 \quad I(ML) = \begin{cases} 0 & ML \leq EX \\ CO \cdot (ML - EX) & EX < ML < INV \\ CO \cdot (INV - EX) & ML \geq INV \end{cases} \quad (21)$$

542 where CO is the co-insurance factor that typically equals to 1.0 for home insurance in Australia,
 543 EX is the excess fee or deductibles, and INV is the insured value of the house. If EX equals to
 544 zero and INV is infinity, $E[I(ML)]$ is the annual expected loss given by Table 8.

545 For a typical building and contents insurance policy for the representative contemporary
 546 house described in Section 4.1 with a EX of \$600, the annual insurance premium INP ranges
 547 from \$1,000 to \$1,500 for houses in Brisbane and \$600 to \$1,000 for houses in Melbourne,
 548 which includes risks from windstorms, theft, impact, earthquake, fire, accidental damage, etc.
 549 The flood coverage is generally optional and not initially included in INP . It is further assumed
 550 that INV is 30% higher than the total building and contents value (i.e. \$375,000 as described in
 551 Section 6). By substituting the random samples of ML yielded by the probabilistic risk
 552 assessment using MCS analysis into Eq. (21), $E[I(ML)]$ is estimated to be \$257 and \$206 for
 553 the Brisbane house with a design wind classification of N2 and N3, respectively. For the
 554 Melbourne house with a design wind classification of N1 and N2, $E[I(ML)]$ is estimated to be
 555 \$76 and \$101, respectively. These estimates seem to be reasonable risk premiums for wind and
 556 rainfall damage compared to the typical INP values for Brisbane and Melbourne houses
 557 including all sources of risks. Incorporating the effects of construction defects can further
 558 increase the estimates. A detailed reality check can be further conducted if the breakdown of a
 559 typical insurance premium for housing (e.g. annual premiums respectively correspond to
 560 distinct natural and man-made hazards) is known.

561 7.2.3. Sensitivity analysis

562 7.2.3.1. *Parameters of rainwater intrusion model*

563 The parameters of the semi-empirical rainwater intrusion model given by Table 5 are
564 subjected to considerable uncertainties due to limited experimental and field monitoring
565 evidence. A sensitivity analysis is conducted by varying the mean values of the parameters in
566 Table 5 by $\pm 50\%$ and adjusting the corresponding standard deviations accordingly to keep the
567 COV values unchanged. Table 10 shows the respective effects of RAF_R , RAF_W , f_v and f_r on the
568 annual expected losses. The variations of the mean RAF_R and f_v have limited effects on the
569 estimated annual expected losses, whereas the risk analysis is relatively sensitive to changes in
570 RAF_W , which indicates that rainwater tends to enter from windward windows. Varying the
571 mean f_r considerably changes the estimated annual expected losses by up to 10%, and hence
572 more detailed evaluation of rainwater runoff by either experiments or numerical methods (e.g.
573 Blocken & Carmeliet 2012; Blocken & Carmeliet 2015) for the building material of the
574 representative contemporary house are needed to better estimate this reduction factor in the
575 future work.

576 7.2.3.2. *Parameters in loss functions*

577 The threshold of water depth h_T leading to a total loss of building interior and contents, and
578 the weighting factor w_0 in Eq. (16) and (17) are varied by $\pm 50\%$. The corresponding changes
579 in the calculated annual expected losses are also shown in Table 10. While the effect of w_0 is
580 negligible, the estimated annual expected losses are very sensitive to a -50% decrease in h_T .
581 This threshold value may depend on the materials of building interior and contents as well as
582 many local factors in pricing and claim evaluation. Hence, a revision of h_T is needed if relevant
583 insurance data in Australia becomes available and accessible.

584 7.2.3.3. *Window size and resistance*

585 A sensitivity analysis suggests that the annual expected losses increase by up to 70% if the

586 windward window area (A_w) is doubled to 8m^2 as also shown in Table 10. Therefore, a
587 contemporary house with a higher window-to-floor ratio (i.e. window area divided by the floor
588 area, typically less than 25% for Australian housing) is more susceptible to wind and rain
589 losses. However, the determination of window-to-floor ratio depends on many other factors
590 such as natural lighting, ventilation, energy efficiency and architectural appearance, etc.

591 The mean window resistances (i.e. R_{ult} and R_{water}) given by Table 1 are varied by $\pm 20\%$.
592 Table 10 shows the sensitivity of the risk analysis to the changes in window resistances. The
593 annual expected losses for Melbourne houses are relatively less sensitive to a 20% change in
594 window resistances and it implies that strengthening windows for housing in Brisbane offers
595 more reduction in economic losses due to extreme wind and associated rainfall.

596 **8. Conclusions and Future Work**

597 In this study, a probabilistic risk assessment framework was developed to evaluate the wind
598 and rain losses for metal-clad houses in non-cyclonic regions of Australia. The components
599 included are (i) a hazard model accounting for the simultaneous occurrence of extreme wind
600 and associated rainfall, (ii) a reliability-based wind damage assessment, (iii) a semi-empirical
601 model for rainwater intrusion, and (iv) a loss estimation model. The risk analysis results suggest
602 that the annual expected losses are mainly attributed to the rainwater damage to building
603 interior and contents. Although houses in Brisbane have a stronger design, they are generally
604 subjected to higher losses than Melbourne houses because the extreme wind speed and
605 associated rainfall intensity are higher in Brisbane.

606 The current risk assessment is conducted for houses with an idealized construction quality.
607 The effect of construction error (e.g. defects in roof connections, the installed window with an
608 unsatisfied window rating) on the economic losses needs to be further investigated. The
609 parameters of the semi-empirical rainwater intrusion model need a revisit when more
610 experimental evidence and CFD studies are available. The threshold of water depth leading to

611 a total loss of building interior and contents used in the loss functions can be further modified
612 when more field observations and insurance data are available. Further decision-analysis for
613 risk mitigation can be conducted based on the probability risk assessment in this study.

614 **Acknowledgement**

615 The first author is supported by the Australian Government Research Training Program
616 Scholarship. The efforts of Dr. Omer Yetemen are greatly appreciated for the discussion and
617 help on the rainfall modelling. The wind and rainfall data for Archerfield airport in Brisbane
618 and Moorabbin airport in Melbourne are provided by the Australian Bureau of Meteorology.

619 **References**

- 620 ABS (2011). *Australian Social Trends December 2011: Components of household wealth*. Australian Bureau of
621 Statistics, Canberra, Australia.
- 622 AS 2047 (2014). *Windows and external glazed doors in buildings*. Standards Australia, Sydney.
- 623 AS 4055 (2012). *Wind Loads for Housing*. Standards Australia, Sydney.
- 624 AS/NZS 1170.2 (2011). *Structural Design Actions, Part 2: Wind Actions*. Standards Australia, Sydney.
- 625 Baheru, T., Chowdhury, A. G., Pinelli, J. P., & Bitsuamlak, G. (2014). Distribution of wind-driven rain deposition
626 on low-rise buildings: Direct impinging raindrops versus surface runoff. *Journal of Wind Engineering and*
627 *Industrial Aerodynamics*, 133, 27-38.
- 628 Baheru, T., Chowdhury, A. G., & Pinelli, J. P. (2015). Estimation of wind-driven rain intrusion through building
629 envelope defects and breaches during tropical cyclones. *Natural Hazards Review*, 16(2), 04014023.
- 630 Blocken, B., & Carmeliet, J. (2002). Spatial and temporal distribution of driving rain on a low-rise building. *Wind*
631 *and Structures*, 5(5), 441-462.
- 632 Blocken, B., & Carmeliet, J. (2004). A review of wind-driven rain research in building science. *Journal of wind*
633 *engineering and industrial aerodynamics*, 92(13), 1079-1130.
- 634 Blocken, B., & Carmeliet, J. (2010). Overview of three state-of-the-art wind-driven rain assessment models and
635 comparison based on model theory. *Building and Environment*, 45(3), 691-703.
- 636 Blocken, B., & Carmeliet, J. (2012). A simplified numerical model for rainwater runoff on building facades:
637 possibilities and limitations. *Building and Environment*, 53, 59-73.
- 638 Blocken, B., & Carmeliet, J. (2015). Impact, runoff and drying of wind-driven rain on a window glass surface:
639 numerical modelling based on experimental validation. *Building and Environment*, 84, 170-180.
- 640 Choi, E. C. C. (1994a). Determination of wind-driven-rain intensity on building faces. *Journal of Wind*
641 *Engineering and Industrial Aerodynamics*, 51(1), 55-69.
- 642 Choi, E. C. C. (1994b). Characteristics of the co-occurrence of wind and rain and the driving-rain index. *Journal*
643 *of wind engineering and industrial aerodynamics*, 53(1-2), 49-62.
- 644 CIBSE (2015). *GVA/15 CIBSE Guide A: Environmental Design 2015*. The Chartered Institution of Building
645 Services Engineers, London, UK.
- 646 CTS (2018). *North Queensland Study into Water Damage from Cyclones*. A summary of report TS1124, Cyclone
647 Testing Station, James Cook University.

- 648 Dao, T. N. (2010). *The development of performance-based wind engineering for residential structures: From*
649 *concept to application*. Ph.D. dissertation, Colorado State University, Fort Collins, CO, USA.
- 650 Dao, T. N., & van de Lindt, J. W. (2010). Methodology for wind-driven rainwater intrusion fragilities for light-
651 frame wood roof systems. *Journal of Structural Engineering*, 136(6), 700-706.
- 652 Eagleson, P. S. (1972). Dynamics of flood frequency. *Water Resources Research*, 8(4), 878-898.
- 653 ESDU (2002). *Strong winds in the atmospheric boundary layer. II: Discrete gust speeds*. Engineering Science
654 Data Unit, Item No. 83045, London, UK.
- 655 Ginger, J., Henderson, D., Edwards, M. and Holmes, J. (2010). Housing damage in windstorms and mitigation
656 for Australia. *Proceedings of 2010 APEC-WW and IG-WRRR Joint Workshop: Wind-Related Disaster Risk*
657 *Reduction Activities in Asia-Pacific Region and Cooperative Actions*, 1-18.
- 658 Goda, K., & Hong, H. P. (2008). Implied preference for seismic design level and earthquake insurance. *Risk*
659 *Analysis: An International Journal*, 28(2), 523-537.
- 660 Hamid, S., Kibria, B. G., Gulati, S., Powell, M., Annane, B., Cocke, S., ... & Chen, S. C. (2010). Predicting losses
661 of residential structures in the state of Florida by the public hurricane loss evaluation model. *Statistical*
662 *methodology*, 7(5), 552-573.
- 663 HAZUS (2014). *Multi-hazard Loss estimation methodology - hurricane model*. Hazus-MH 2.1 Technical Manual,
664 Federal Emergency Management Agency, Mitigation Division, Washington, DC.
- 665 Henderson, D. J., & Ginger, J. D. (2007). Vulnerability model of an Australian high-set house subjected to
666 cyclonic wind loading. *Wind and Structures*, 10(3), 269-285.
- 667 Henderson, D., & Ginger, J. (2008). Role of building codes and construction standards in windstorm disaster
668 mitigation. *Australian Journal of Emergency Management*, 23(2), 40-46.
- 669 Henderson D, Smith D, Boughton G, Falck D and Ginger J (2017). Damage and losses in engineered buildings
670 from wind and rain. *24th Australasian Conference on the Mechanics of Structures and Materials*. 6-9 December
671 2016, Perth, Australia.
- 672 Heneker, T. M., Lambert, M. F., & Kuczera, G. (2001). A point rainfall model for risk-based design. *Journal of*
673 *Hydrology*, 247(1-2), 54-71.
- 674 HIA (2018). *Window into Housing 2018*. The Housing Industry Association, Canberra, Australia.
- 675 ISO (2009). *Hygrothermal performance of buildings – calculation and presentation of climatic data – Part 3:*
676 *calculation of a driving rain index for vertical surfaces from hourly wind and rain data*. International Organization
677 for Standardization 2009, 15927-3.
- 678 Johnson, T., Pinelli, J. P., Baheru, T., Chowdhury, A. G., Weekes, J., & Gurley, K. (2018). Simulation of Rain
679 Penetration and Associated Damage in Buildings within a Hurricane Vulnerability Model. *Natural Hazards*
680 *Review*, 19(2), 04018004.
- 681 Koutsoyiannis, D., & Foufoula-Georgiou, E. (1993). A scaling model of a storm hyetograph. *Water Resources*
682 *Research*, 29(7), 2345-2361.
- 683 Koutsoyiannis, D., Onof, C., & Wheeler, H. S. (2003). Multivariate rainfall disaggregation at a fine timescale.
684 *Water Resources Research*, 39(7).
- 685 Lambert, M., & Kuczera, G. (1998). Seasonal generalized exponential probability models with application to
686 interstorm and storm durations. *Water Resources Research*, 34(1), 143-148.
- 687 Leitch C, Ginger J, Harper B, Kim P, Jayasinghe N, Somerville L (2009). *Investigation of performance of housing*
688 *in Brisbane following storms on 16 and 19 November 2008*, Technical Report No. 55. Cyclone Testing Station,
689 James Cook University.
- 690 Li, Y., van de Lindt, J. W., Dao, T., Bjarnadottir, S., & Ahuja, A. (2011). Loss analysis for combined wind and
691 surge in hurricanes. *Natural hazards review*, 13(1), 1-10.
- 692 Mudd, L., Rosowsky, D., Letchford, C., & Lombardo, F. (2016). Joint Probabilistic Wind–Rainfall Model for
693 Tropical Cyclone Hazard Characterization. *Journal of Structural Engineering*, 143(3), 04016195.

- 694 Pant, S., & Cha, E. J. (2019). Wind and rainfall loss assessment for residential buildings under climate-dependent
695 hurricane scenarios. *Structure and Infrastructure Engineering*, 15(6), 771-782.
- 696 Parackal, K. I., Humphreys, M. T., Ginger, J. D., & Henderson, D. J. (2016). Wind Loads on Contemporary
697 Australian Housing. *Australian Journal of Structural Engineering*, 17(2), 136-150.
- 698 Pita, G., Pinelli, J. P., Cocke, S., Gurley, K., Mitrani-Reiser, J., Weekes, J., & Hamid, S. (2012). Assessment of
699 hurricane-induced internal damage to low-rise buildings in the Florida Public Hurricane Loss Model. *Journal of*
700 *Wind Engineering and Industrial Aerodynamics*, 104, 76-87.
- 701 Porter, K. A., Kiremidjian, A. S., & LeGrue, J. S. (2001). Assembly-based vulnerability of buildings and its use
702 in performance evaluation. *Earthquake spectra*, 17(2), 291-312.
- 703 Qin, H., & Stewart, M. G. (2019). System fragility analysis of roof cladding and trusses for Australian
704 contemporary housing subjected to wind uplift. *Structural Safety*, 79, 80-93.
- 705 R Core Team (2019). *R: A language and environment for statistical computing*. R Foundation for Statistical
706 Computing, Vienna, Austria. URL: <http://www.R-project.org/>.
- 707 Rawlinsons (2015). *Rawlinsons Construction Cost Guide 2015*. Rawlinsons Publishing, Perth, Australia.
- 708 RLB (2019). *Riders Digest 47th Edition*. Rider Levett Bucknall, Australia.
- 709 Smith, D., & Henderson, D. (2015). *Suncorp group limited: Cyclone resilience research – Phase II*. Report
710 TS1018, Cyclone Testing Station, James Cook University, Australia.
- 711 Stewart, M. G., Ginger, J. D., Henderson, D. J., & Ryan, P. C. (2018). Fragility and climate impact assessment of
712 contemporary housing roof sheeting failure due to extreme wind. *Engineering Structures*, 171, 464-475.
- 713 Straube, J. F., & Burnett, E. F. P. (2000). Simplified prediction of driving rain on buildings. *Proceedings of the*
714 *international building physics conference*. Eindhoven, Netherlands.
- 715 van de Lindt, J. W., & Nguyen Dao, T. (2012). Loss analysis for wood frame buildings during hurricanes. II: Loss
716 estimation. *Journal of performance of constructed facilities*, 26(6), 739-747.
- 717 Walker, G. R., Mason, M. S., Crompton, R. P., & Musulin, R. T. (2016). Application of insurance modelling tools
718 to climate change adaptation decision-making relating to the built environment. *Structure and Infrastructure*
719 *Engineering*, 12(4), 450-462.
- 720 Wang, C. H., Wang, X., & Khoo, Y. B. (2013). Extreme wind gust hazard in Australia and its sensitivity to climate
721 change. *Natural hazards*, 67(2), 549-567.
- 722

723 **Tables**

724 Table 1. Ultimate strength and water penetration resistance of windows.

Window rating	R_{ult} (Pa)		R_{water} (Pa)		Distribution type
	Mean	COV	Mean	COV	
N1	720	0.20	180	0.20	Normal
N2	1080	0.20	180	0.20	
N3	1680	0.20	360	0.20	

725
726
727

Table 2. Limit states for the windward window.

Limit states	Internal pressurisation scenario	Water entry
$W_{win} \geq R_{ult}$	Windward dominant opening	Via window breakage
$W_{win} \geq R_{water} \cap W_{win} < R_{ult}$	No dominant opening	Via small gaps around the window
$W_{win} < R_{water}$	No dominant opening	No entry via window

728
729
730
731
732
733
734

Table 3. DRF values corresponding to various rainfall intensities.

R_h (mm/hr)	10	20	30	40	50	60	80	100
DRF	0.209	0.186	0.175	0.168	0.163	0.159	0.153	0.149

735 Table 4. Gust factors corresponding to different averaging periods (gust duration of 0.2s).

Averaging periods (hr)	0.5	1	2	3	6	9	12	18	24
Gust factor (G_u)	1.73	1.77	1.80	1.82	1.85	1.87	1.88	1.90	1.91

736
737
738

Table 5. Random variables in the semi-empirical rainwater intrusion model.

Parameters	Location applied	Mean	Standard deviation	Distribution	Source
RAF_R	Windward roof	0.30	0.20	Truncated normal ^a	Inferred from Baheru et al. (2014)
	Sideward roof	0.05	0.05		
	Leeward roof	0.00	0.00		
RAF_W	Windward window	0.50	0.20	Truncated normal ^a	Inferred from Straube & Burnett (2000) Baheru et al. (2014)
f_v	Gaps around windward window	2.50	0.30	Truncated normal ^a	Inferred from CIBSE (2015)
f_r	Upstream undamaged surface	0.25	0.15	Truncated normal ^a	Assumed based on engineering judgement

739 ^aTruncated to an interval of 0 to 1.

740

741

Table 6. Subassembly cost ratios for the representative contemporary house.

Subassembly		Description	Cost ratio	Adjusted cost ratio
Roof	Roof cladding	Mainly including corrugated metal sheets, metal battens and insulation	4.1%	$L_1 = 5.4\%$
	Roof framing	Timber trusses, rafters, ceiling joists, fixings, etc.	15.9%	$L_2 = 20.9\%$
Windows on one wall		Single glazed, aluminum sliding or awning windows	0.8%	$L_3 = 1.0\%$
Internal finishes, fittings	Wall	Mostly plasterboard, also include ceramic tiles and painting	6.8%	$L_4 = 51.2\%$ (building interior)
	Floor	Mixed use of timber, carpet and ceramic tiles	3.5%	
	Ceiling	Mostly plasterboard, also including painting	4.7%	
	Fittings and fixtures	Built-in wardrobes/cupboards, kitchen units, bathroom suites, shelving, internal doors, etc.	10.0%	
Mechanical		Air conditioning, heaters, ventilation, etc.	10.0%	
Electrical		Lighting, conduits, cables, etc.	4.0%	
Other		Site preparation, foundation, wall framing, other fenestrations, plumbing, etc.	37.0%	n/a

742

743

744

Table 7. Nominal values of T and D for suburban houses with different design wind classifications.

	Design wind classification	T_N	D_N
Brisbane house	N2	0.90	1.0
	N3	1.0	1.0
Melbourne house	N1	0.90	See Table 3.2 in AS/NZS 1170.2 (2011)
	N2	1.0	

745

746

747

Table 8. Annual expected losses for the representative contemporary house.

	Design wind classification	Annual expected loss (%)						Loss of use (days)	Portion of window breakage (%)
		L_1	L_2	L_3	L_4	L_5	Total		
Brisbane	N2	0.004	0.003	0.003	0.069	0.030	0.109	0.22	0.27
	N3	0.006	0.002	0.001	0.053	0.023	0.085	0.17	0.07
Melbourne	N1	0.000	0.000	0.000	0.024	0.011	0.035	0.04	0.009
	N2	0.000	0.000	0.000	0.032	0.014	0.046	0.06	0.006

748

749 Table 9. Mean damage states under extreme wind speed with 50 and 500 year return periods.

	Design wind classification	V ₅₀			V ₅₀₀		
		R _{clad} (%)	R _{truss} (%)	h _l (mm)	R _{clad} (%)	R _{truss} (%)	h _l (mm)
Brisbane house	N2	0.00	0.00	0.10	0.73	1.01	0.22
	N3	0.00	0.00	0.08	1.22	0.56	0.16
Melbourne house	N1	0.00	0.00	0.02	0.00	0.00	0.04
	N2	0.00	0.00	0.03	0.00	0.00	0.05

750

751

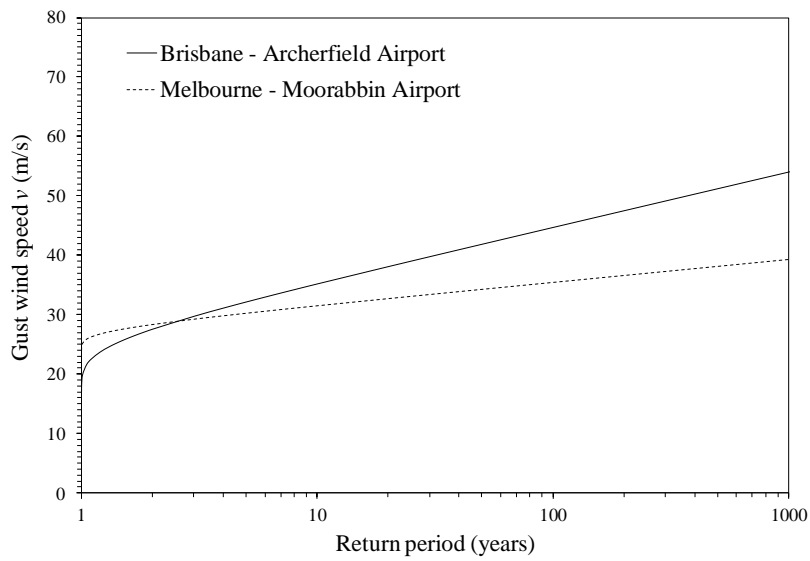
752 Table 10. Sensitivity of annual expected losses to various uncertain parameters.

Parameters	Variations for sensitivity analysis	Approximate changes in annual expected losses	
		Brisbane house	Melbourne house
RAF_R		±5%	±5%
RAF_W	±50% of the mean values given in Table 5 and COV values unchanged	±30%	±30%
f_v		±1%	±1%
f_r		±10%	±10%
h_T	±50% of the values given in Section 6.2.4 and 6.2.5	-30% and +60%	-30% and +70%
w_0		±1%	±1%
A_W	Doubled to 8m ²	+70%	+70%
R_{ult} and R_{water}	±20% of the mean window resistances given in Table 1	-20% and +25%	-10% and +15%

753

754

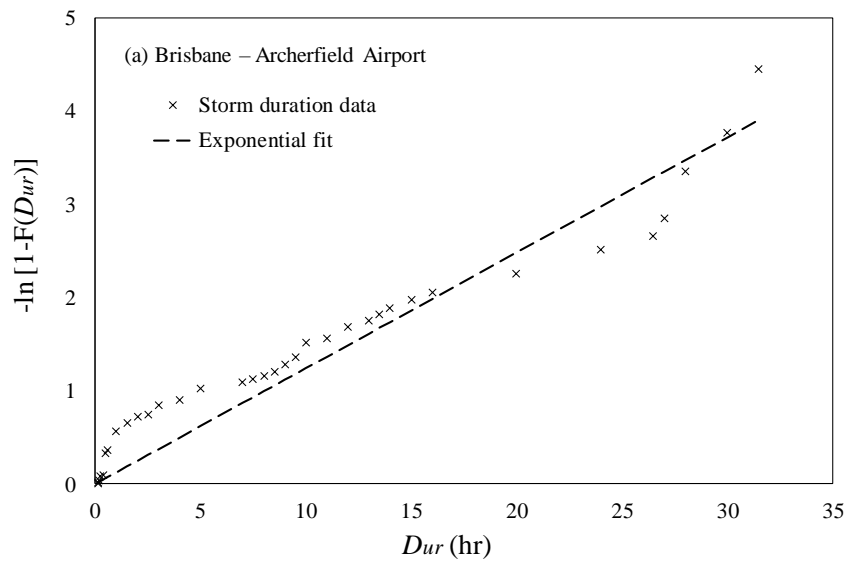
755 **Figures**



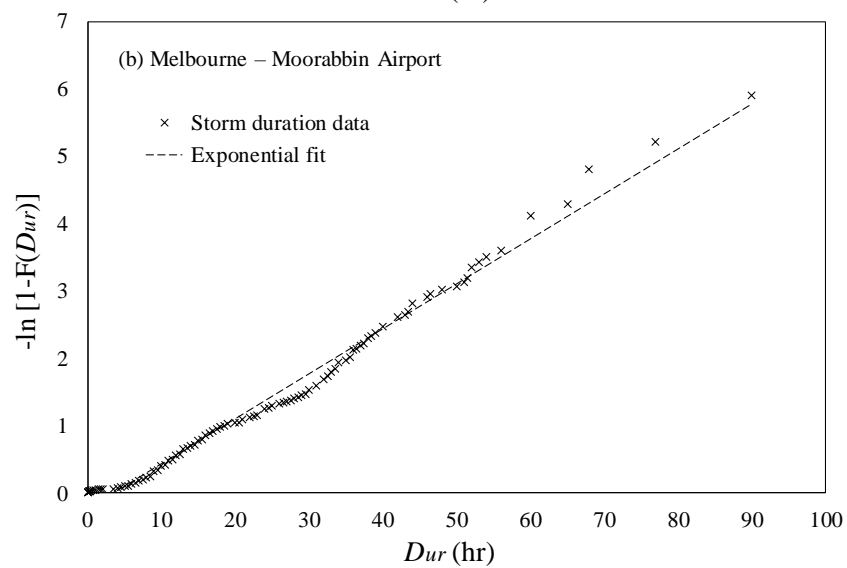
756

757

Figure 1. Extreme gust wind speed corresponding to return periods.



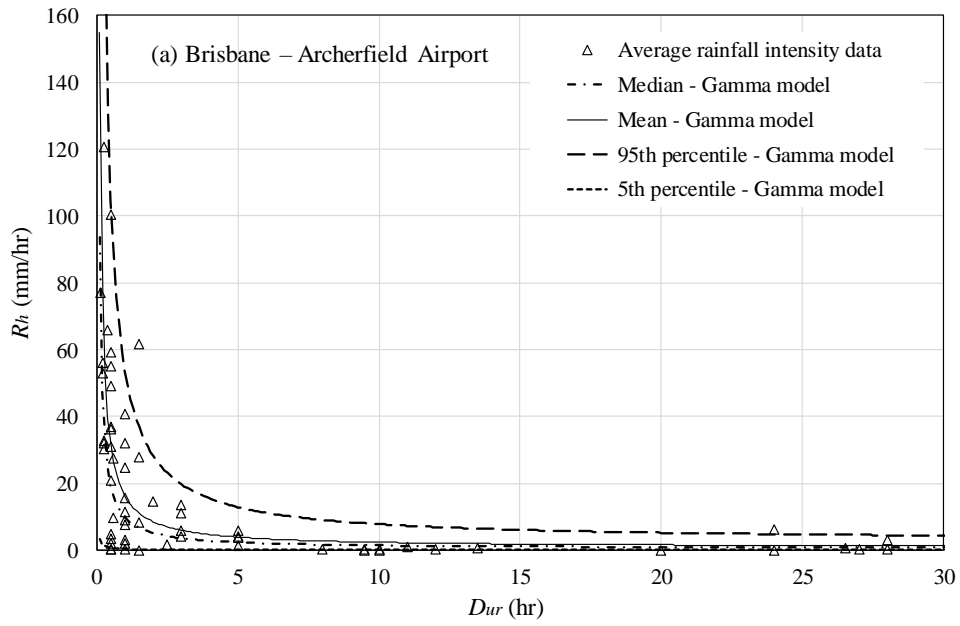
758



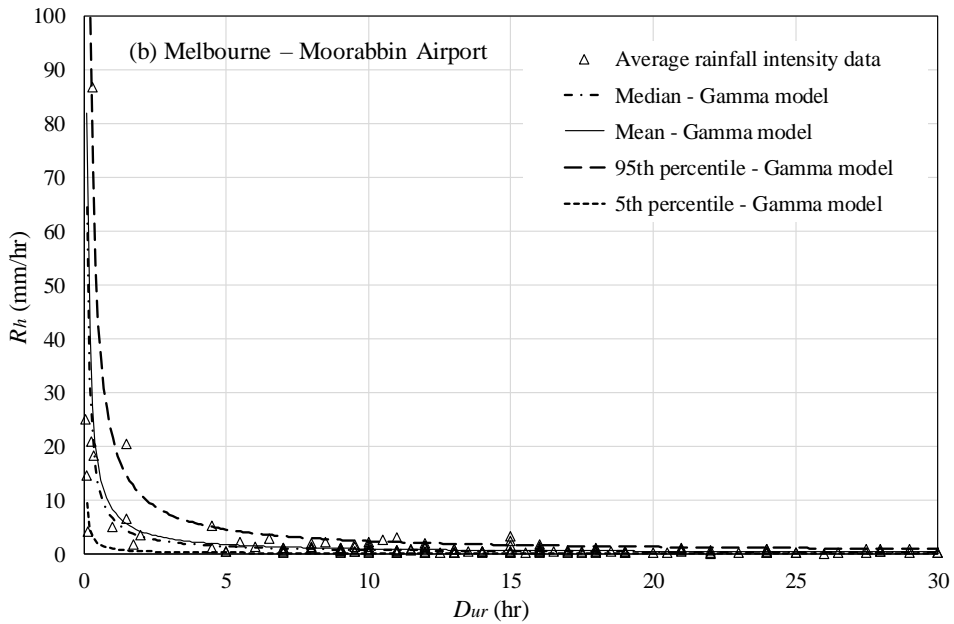
759

760

Figure 2. Exponential probability plots for storm duration D_{ur} .



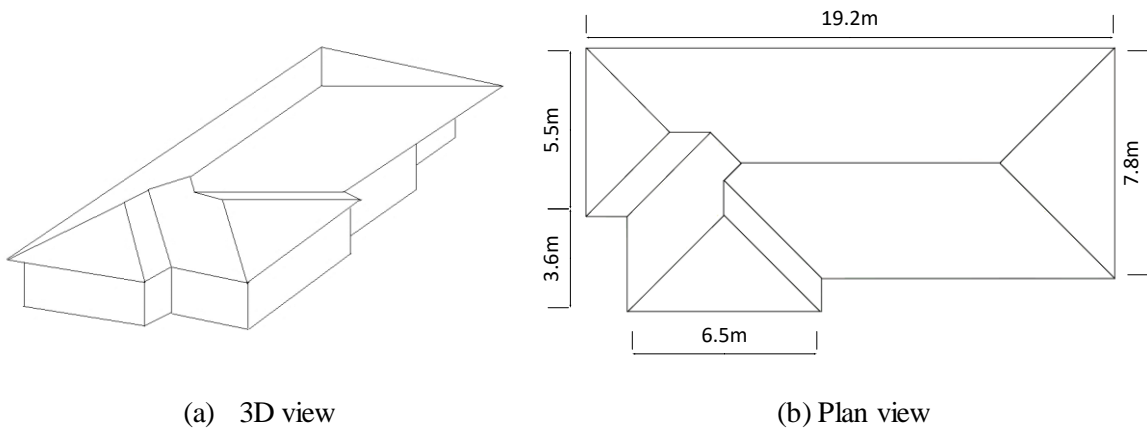
761



762

763

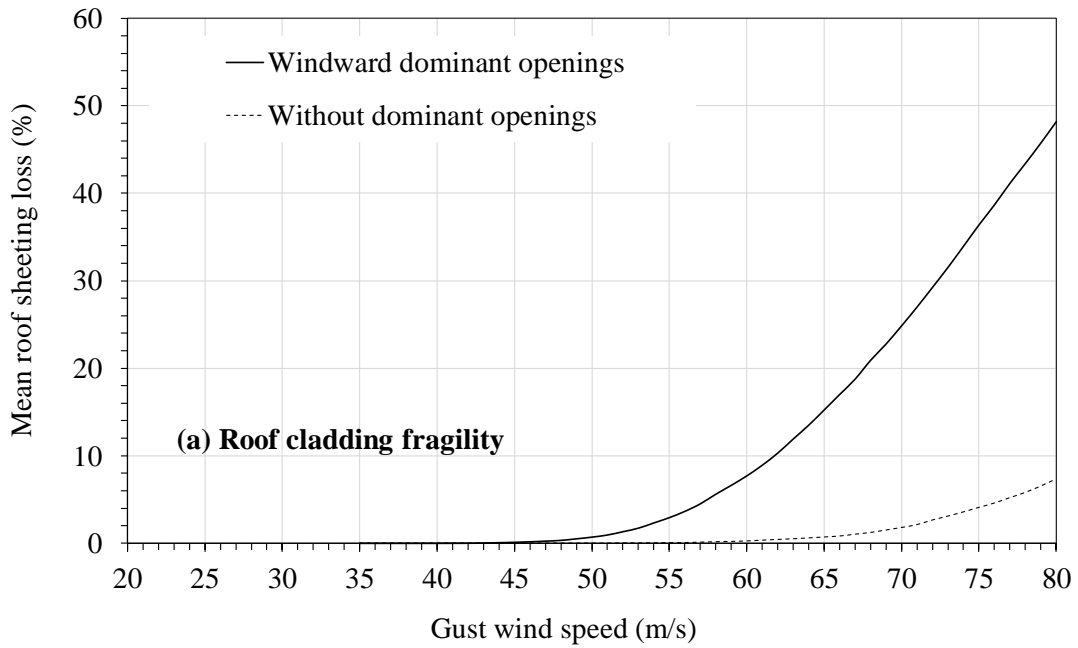
Figure 3. Average rainfall intensity R_t from the observed data and gamma regression model.



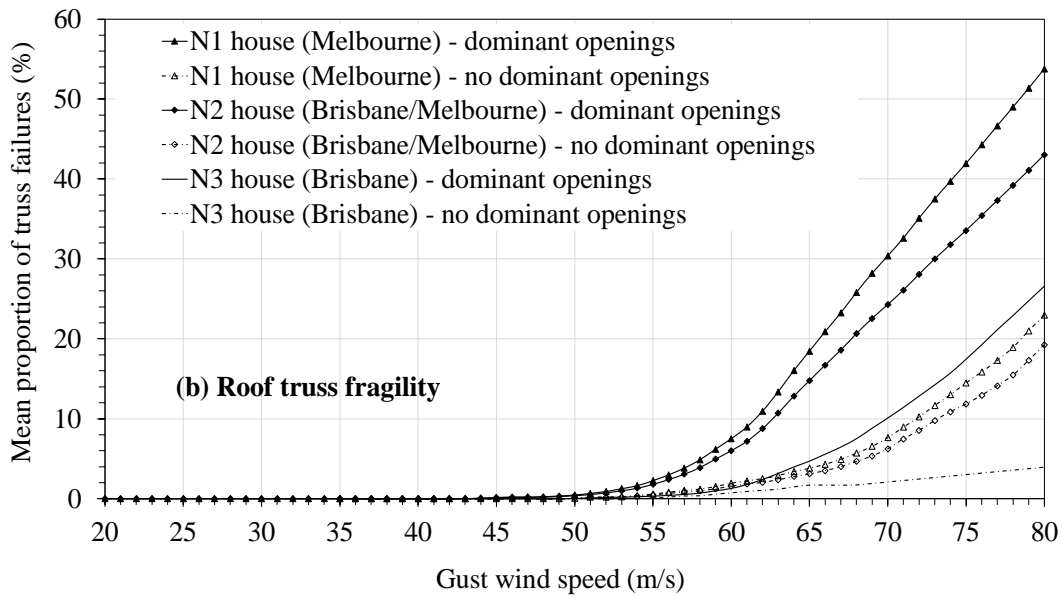
764

765

Figure 4. One-storey representative contemporary house.



766

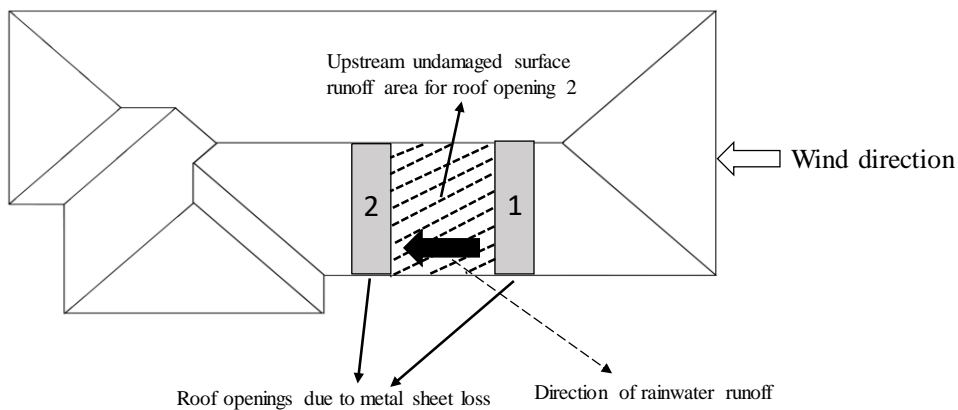


767

768

769

Figure 5. Fragility curves for metal roof cladding and timber roof trusses.

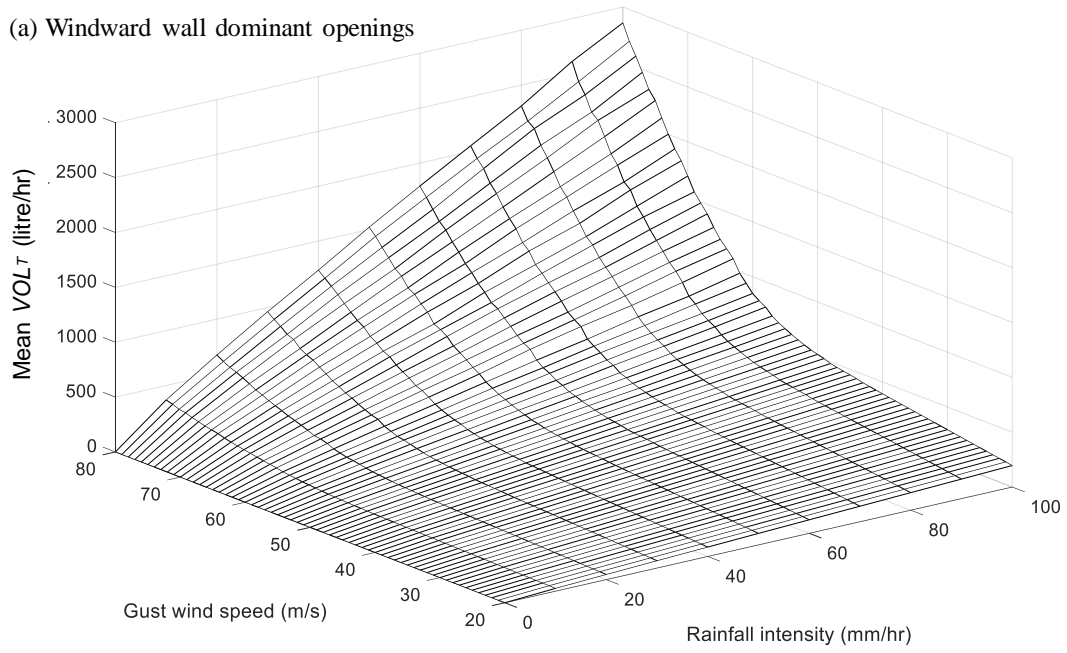


770

771

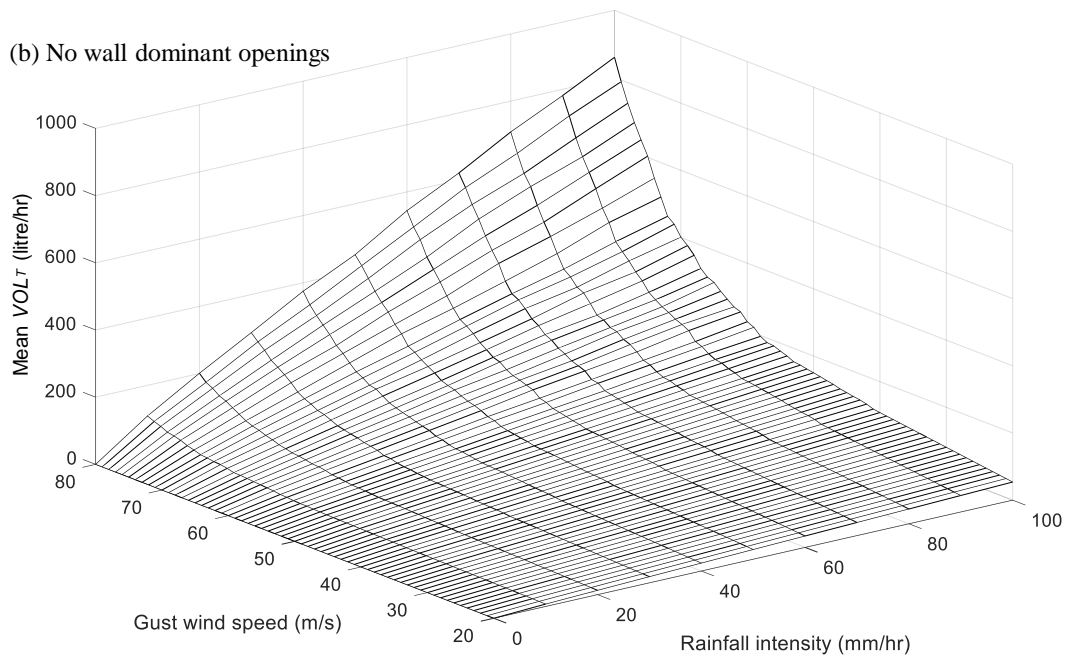
Figure 6. Upstream undamaged surface runoff area for a roof opening due to metal sheet loss.

(a) Windward wall dominant openings



772
773
774

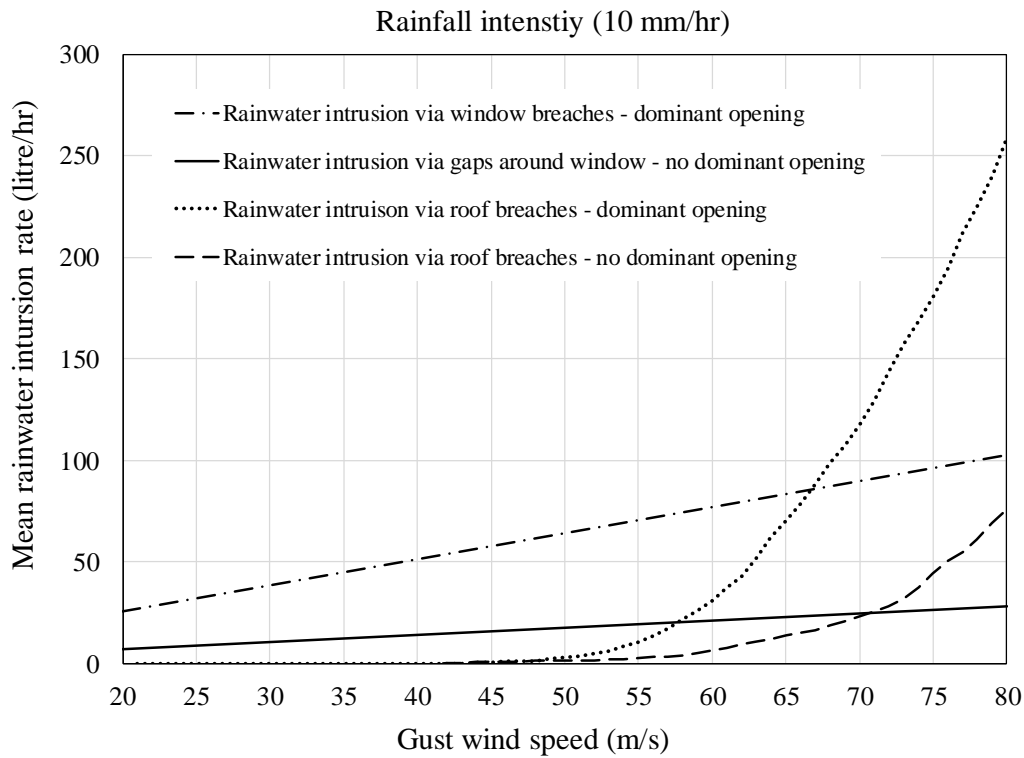
(b) No wall dominant openings



775
776

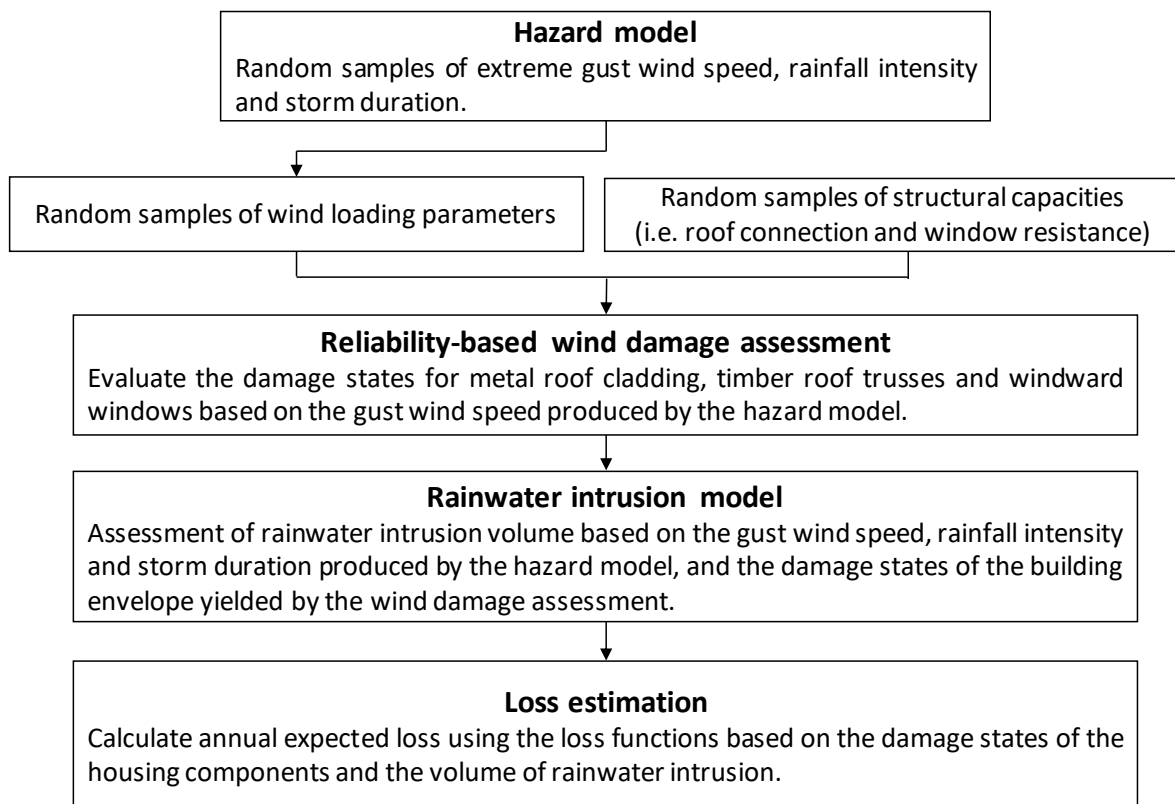
777

Figure 7. Mean VOL_T for two wall opening scenarios.



778
779
780

Figure 8. Mean volumetric rate of rainwater intrusion via roof and window respectively under the two wall opening scenarios at a rainfall intensity of 10 mm/hr.



781
782

Figure 9. Outline of the risk analysis method.